An Experimental and Theoretical Study of Laser Postionization of Femtosecond Laser Desorbed Drug Molecules

Cornelius L. Pieterse, Ivan Rungger, and Ian S. Gilmore
National Physical Laboratory, Hampton Road, Teddington, TW11 0LW UK
Raveendra C. Wickramasinghe and Luke Hanley*
Department of Chemistry, University of Illinois at Chicago, Chicago, IL 60607 USA

Abstract

Femtosecond laser desorption postionization mass spectrometry using 7.9 eV single photon ionization (7.9 eV fs-LDPI-MS) detected three of four drug compounds previously found to have very low ionization efficiencies by secondary ion mass spectrometry (SIMS). Electronic structure calculations of the ionization energies and other properties of these four drug compounds predicted that all display ionization energies below the 7.9 eV photon energy, as required for single photon ionization. The 7.9 eV fs-LDPI-MS of carbamazepine, imipramine, and verapamil all showed significant precursor (M^+) ion signal, but no representative signal was observed for ciprofloxacin. Furthermore, 7.9 eV fs-LDPI-MS displayed higher M^+ signal and mostly similar fragment ions compared to 70 eV electron impact mass spectra. Ionization and fragmentation patterns are discussed in terms of calculated wavefunctions for the highest occupied molecular orbitals. The implications for improving lateral resolution and sensitivity of MS imaging of drug compounds are also considered.

*Corresponding author email: LHanley@uic.edu, +1-312-996-0945, LH ORCID: 0000-0001-7856-1869

CLP ORCID: 0000-0001-5014-0173

IR ORCID: 0000-0002-9222-9317

ISG ORCID: 0000-0002-0981-2318

RCW ORCID: 0000-0001-9371-9839

A major challenge for the pharmaceutical industry is to reduce drug attrition, the failure of a candidate drug molecule along the decade-long development path to become a medicine.[1] These failures, especially at late-stage, drive up the cost of developing a new medicine to approximately $2B. It is of critical importance to identify potential failures at as early a stage as possible[2] and mass spectrometry (MS) imaging is used to examine whether the drug reaches the right biological target and has the right functional pharmacological activity. There is an increasing need to image with sub-cellular spatial resolution[3] and this demands higher sensitivity. One action to reduce drug attrition has been to improve the solubility of drugs and many are now designed to be more hydrophilic (i.e., displaying a partition coefficient, P, between different solvents such that Log P < 3).[4]

Secondary ion mass spectrometry (SIMS) uses a focused ion beam as the sputtering probe for MS imaging of drugs and their metabolites in tissue[4] as well as other applications.[5,6] Unfortunately, the ionization process in SIMS is not very efficient, with only ~1 in 10^4 molecules typically ionized and detected.[5,6] Furthermore, the sensitivity of SIMS has been found to be inversely proportional to Log P so that many drug compounds of importance to industry are either difficult or impossible to detect via SIMS.[4]

Prior work has demonstrated that the ionization efficiency in SIMS (as well as in laser desorption-based MS imaging) can be increased by over 100-fold using single photon ionization or other laser postionization schemes.[6-9] The 7.9 eV (157 nm) output of the fluorine excimer laser is perhaps the lowest cost, highest repetition rate, and experimentally most robust strategy for laser-based single photon ionization, making it attractive for enhancing signal in SIMS.[10]

7.9 eV single photon ionization has also been coupled to nanosecond laser desorption,[11-14] even detecting molecules larger than 10,000 Da.[15] Laser-based single photon ionization has more

recently been combined with femtosecond laser desorption (fs-LD) at the University of Illinois at Chicago (UIC) for MS imaging of molecular species in biofilms[9,16] with near-micron lateral resolution (as measured on test samples).[17] However, those experiments were experimentally inconvenient as single photon ionization was accomplished with the low intensity and low repetition rate 10.5 eV (118 nm) pulses generated from the ninth harmonic of the Nd:YAG laser.[8,14]

Femtosecond laser desorption postionization mass spectrometry using 7.9 eV single photon ionization (7.9 eV fs-LDPI-MS) is explored here for the detection of four drug compounds that have previously been found to have very low ionization efficiencies in SIMS: carbamazepine, ciprofloxacin, verapamil, and imipramine, whose Log P values range from -0.81 to 5.23.[4] 7.9 eV fs-LDPI-MS successfully detected carbamazepine, verapamil, and imipramine. At least two micrometer lateral resolution MS imaging of these compounds should be possible with fs-LDPI-MS, when prior work is taken into account.[17] Electronic structure calculations indicated that all four compounds have sufficiently low ionization energies to undergo 7.9 eV single photon ionization, although no experimental signal was observed for ciprofloxacin. Finally, 7.9 eV fs-LDPI-MS is shown to compare advantageously to SIMS and traditional 70 eV electron impact mass spectra.

Laser desorption was performed here using ~75 fs, 800 nm laser pulses from a compressed pulse fs laser system (Tsunami master oscillator pumped by Millenia Vs and Spitfire amplifier pumped by Evolution-30, Spectra Physics, Irvine, CA). The Gaussian shaped fs-laser pulse was converted into a flat-top intensity profile by Pi-shaper optics, then focused (NA 0.28, Mitutoyo, Japan) to a 20 × 10 μm elliptical laser spot.[18] 7.9 eV single photon ionization was performed using a fluorine excimer laser that outputs ~7 ns, 157 nm pulses (EX5AF/250, GAM laser, Orlando, FL, USA). The postionization laser pulse was fired ~1.8 μs after the desorption laser pulse, with both

lasers operating at a 100 Hz repetition rate and the sample stage rastered in a z-pattern at a speed of 1 mm/s. The ion source of the fs-LDPI mass spectrometer is shown schematically in Figure 1 whereas its sample motion stage, ion detection, and data analysis software were described previously.[17,19] Ion acceleration was 4 keV, achieved by pulsing the sample stage. The mass analyser has recently been updated with a unique reflectron time-of-flight mass analyser consisting of two right angle ion mirrors installed with an intermediate, adjustable slit and various Einzel and steering lenses.[20,21]

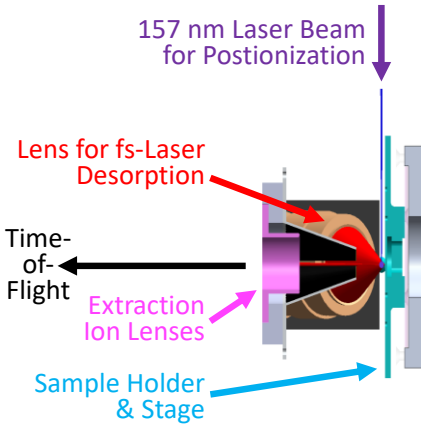

Figure 1. *Schematic diagram of source region of femtosecond laser desorption postionization mass spectrometer (fs-LDPI-MS). Ions formed by 75 fs, 800 nm pulsed fs-laser desorption via a focusing optic (red) from sample holder (blue) on a moving sample stage (grey) are single photon ionized by a 157 nm (7.9 eV) laser beam (purple) then accelerated into a time-of-flight mass analyser.*

The lowest laser desorption fluence value was selected to be approximately at threshold for the observation of postionization. The entire area associated with each sample was scanned for fluence values ranging from the minimum to a predefined maximum. For each scan, the pulse energy was increased by 1 uJ until a total of four data points were acquired. Approximately 1600 representative spectra (those for which the intact precursor ion or its fragments were detected) were included in each average. The use of threshold laser desorption fluence as well as the uneven distribution of drug compound across the targe surface led to the rejection of ~80% (~6500) of all

collected spectra for each sample because they displayed no significant precursor or fragment ion signal. No signal was observed for either fs-laser desorption ionization or 7.9 eV laser postionization alone (see Supporting Information, Figure S1).

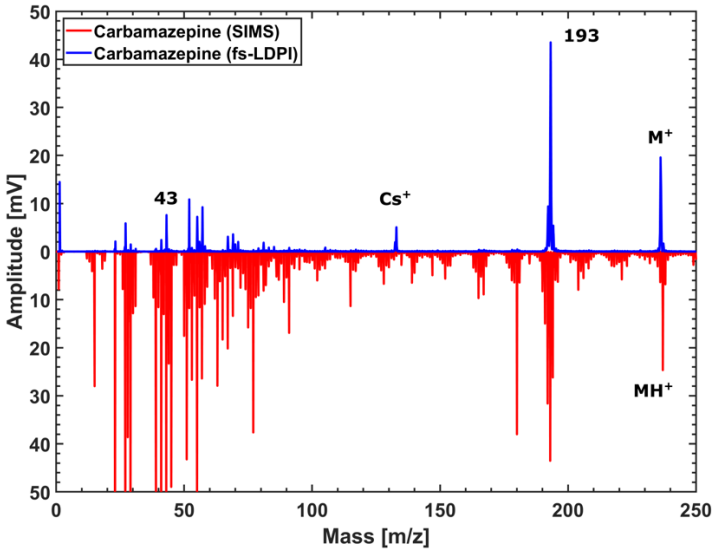

***Figure 2**. 7.9 eV fs-LDPI-MS of carbamazepine, compared with the previously reported 25 keV Bi_3^+ secondary ion mass spectrum.[4] SIMS data normalized to 50 mV (near maximum of fs-LDPI mass spectra).*

Previously reported SIMS data[4] is compared in Figure 2 with the 7.9 eV fs-LDPI-MS data for carbamazepine. The carbamazepine SIMS was recorded[4] with 13 ns pulses of 25 keV Bi_3^+ primary ions focussed into a ~2 µm diameter beam with an average current of 0.1 pA, corresponding to a dose of 9×10^{12} ions/cm^2. The comparison of carbamazepine detection in Figure 2 indicates that 7.9 eV fs-LDPI produces much simpler mass spectra with less chemical noise than SIMS. The most significant fragment ions observed by SIMS are similar to those of fs-LDPI-MS, but SIMS displayed a more complex fragmentation pattern overall than fs-LDPI-MS. The fs-LDPI-MS displays an intact M^+ precursor radical cation at m/z 236 while the SIMS displays the MH^+ ion as well as many other peaks likely arising from proton transfer to or from intact carbamazepine or its fragments. Further comparison of ion sputtering vs. fs-laser desorption is beyond the scope

of this Letter, although a brief examination of fs-laser desorption parameters and their effects upon fs-LDPI-MS is provided in Figures S2 and S3. An insufficient number of compounds were analysed here to draw any conclusions correlating positive ion signal from 7.9 eV fs-LDPI-MS with log P values, as was done previously for SIMS.[4] However, these results (as well as those presented below) support prior studies showing that 7.9 eV laser postionization can also be used to improve on SIMS by the detection of sputtered neutrals.[10]

An obvious disadvantage is that 7.9 eV single photon ionization only occurs for molecules with relatively low ionization energies (IEs).[10-14] The IEs for all four drug molecules studied were therefore calculated to determine the feasibility of ionization in the gas-phase. Density functional theory (DFT) calculations were performed using the SIESTA code[22] with a linear combination of atomic orbitals as the basis set. A double-ζ plus polarisation basis set was used here, with the orbital cut-off determined by an equivalent energy shift of 2.7 meV. This gives rather long basis orbitals that are required to obtain reliable IEs. The calculations were performed within the local density approximation (LDA) for the exchange and correlation functional, as well as within the generalized gradient approximation (GGA). The SIESTA DFT code allows only simulations for periodic systems. It was verified that for the used simulation cubic cell with 40 Å lateral dimension the energies of the molecules converged and did not change upon further increase of the simulation box size. The simulations therefore effectively gave the results for single isolated molecules. The cubic shape of the unit cell also allowed application of the Madelung energy correction for the charged molecule. The real space mesh was set by an equivalent energy mesh cut-off of 300 Ry. For the structural relaxations, all forces were allowed to converge to below 0.04 eV/Å. The so-called Delta-SCF scheme was used to evaluate the vertical IEs as the difference between the total

energy of the singly positively charged molecule and that of the neutral molecule. This method was shown to give IE values usually in good agreement with experiment for organic molecules.[23]

Table 1 reports that the calculated vertical and adiabatic IEs of all four molecules were less than the 7.9 eV photon energy. Such low IEs are expected because all of these molecules have an aromatic chromophore. While all four molecules are therefore expected to undergo threshold single photon ionization, positive ion signal for only three of the four molecules was observed experimentally by 7.9 eV fs-LDPI-MS (no negative ion detection was attempted). None of these molecules were ionized directly during the fs-laser desorption step nor did they sublime at a sufficient rate in the absence of fs-laser desorption to lead to observable 7.9 eV laser postionization signal (see Figure S1).

Table 1. *Vertical and adiabatic ionization energies (IEs) for all four molecules, calculated either within the LDA or the GGA approximation for the exchange correlation potential (units in eV).*

Molecule	**LDA (vertical)**	**LDA (adiabatic)**	**GGA (vertical)**	**GGA (adiabatic)**
Carbamazepine	7.73	7.47	7.50	7.29
Ciprofloxacin	7.49	7.30	7.29	7.12
Verapamil	6.90	6.70	6.66	6.54
Imipramine	6.76	6.66	6.43	6.39

Ciprofloxacin was the only molecule of the four that could not be detected by 7.9 eV fs-LDPI-MS, even though its 7.49 eV vertical IE was calculated to fall well below the 7.9 eV photon energy. Attempts were made here to analyse ciprofloxacin with various measurement strategies, but no 7.9 eV fs-LDPI mass spectrum was observed that was representative of its molecular structure. For example, the laser desorption fluence was increased from the typical 1.1×10^{13} W/cm^2 value to 1.8×10^{13} W/cm^2, but this only enhanced signal from the stainless-steel substrate. The lack of representative ciprofloxacin signal could be explained by a true IE above the 7.9 eV photon energy or dissociation during fs-LD into fragments whose individual IEs

exceed the photon energy. Ciprofloxacin could alternatively be postulated to have undergone extreme dissociation during 7.9 eV single photon ionization, but this seems unlikely given the relatively small excess internal energy expected to be available from fs-LDPI-MS.

Figure 3 shows the highest occupied molecular orbitals (HOMOs) for each of the four neutral molecules, all obtained with GGA. Single photon ionization near the IE threshold is generally expected to occur predominantly from the HOMOs of each of these molecules. The HOMO for carbamazepine is delocalized across much of the fused ring system. The HOMO for imipramine is delocalized across one of the outer rings and the central ring amine, with some electron density residing on the other outer ring. However, ciprofloxacin, carbamazepine and verapamil each display at least two other occupied molecular orbitals within ~0.5 eV (see Table S1 in Supporting Information). These other states generally have different wavefunction distributions. For example, Figure 3 displays the HOMO and the next two occupied molecular orbitals for verapamil (denoted HOMO-1 and HOMO-2). These three states were calculated to be particularly close in energy, so single photon ionization could have occurred from any of them. HOMO-2 is clearly located on one of the phenyl rings, while HOMO and HOMO-1 are located on the amine and the other phenyl ring. GGA generally tends to underestimate the energy difference between states, so that the lower lying HOMOs likely reside at lower energies. Nevertheless, single photon ionization can potentially also occur through at least some of these lower lying molecular states for carbamazepine and verapamil (and in principle, ciprofloxacin, although it displayed no experimental signal). The situation for imipramine might be slightly different as there is only one additional occupied molecular orbital calculated within ~0.5 eV of the HOMO (see Table S1 in Supporting Information). Single photon ionization of lower lying molecular states is further

supported by the general observation that cross sections for single photon ionization increase rapidly with photon energy beyond the IE threshold.[24]

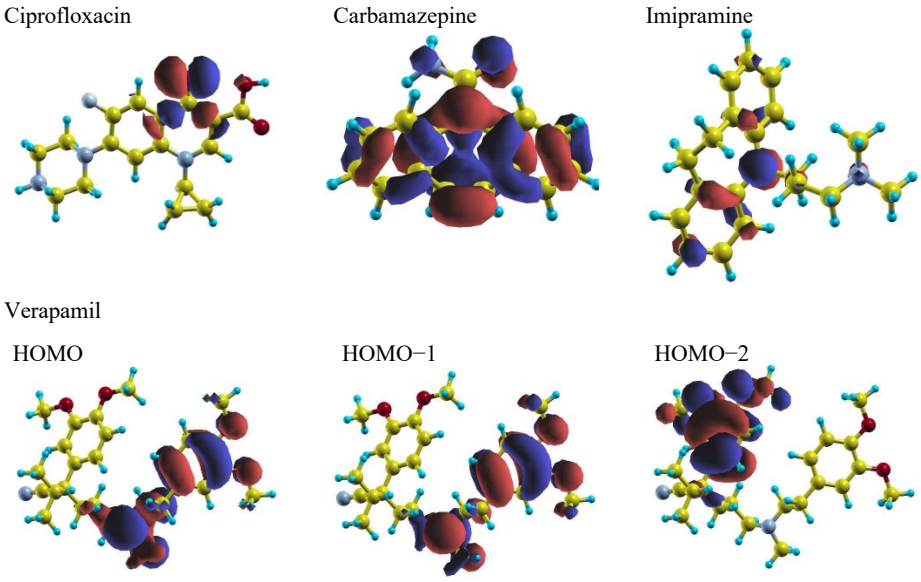

Figure 3. *Top row: Highest occupied molecular orbitals (HOMOs) of ciprofloxacin, carbamazepine, and imipramine. Bottom row: Calculated three highest energy HOMOs of neutral verapamil (see text). C atoms are yellow, H are blue/green, O are grey, and N are red. The wave functions of the HOMO states are plotted as red (positive values) and blue (negative values) isosurfaces.*

The fs-LDPI- and EI-mass spectra for the three detected drug compounds are compared side-by-side in Figure 4. EI-mass spectra were extracted from the NIST Standard Reference Database (NIST Chemistry WebBook, NIST Mass Spectrometry Data Center, webbook.nist.gov/chemistry). The EI-mass spectra were binned at integer mass-to-charge values in the NIST library, then aligned for direct comparison with the fs-LDPI-MS. One of the most striking observations is that the fs-LDPI mass spectra for carbamazepine, imipramine, and verapamil shown in Figure 4 all display many major fragment ions that are also present in their 70 eV electron impact (EI) mass spectra. Furthermore, the highest mass ion in the fs-LDPI-MS is always that of the M^+ precursor radical cation, which is always less intense or absent in the corresponding EI-mass spectra. To further assist in the fragmentation analysis, Figure 5 shows the

real space change in the charge density calculated when one electron is removed from each neutral molecule to form the radical cation that is the precursor ion. Each molecule's fragmentation pathway by fs-LDPI-MS is discussed below along with how it compares with its corresponding EI-mass spectra.

Figure 4(a) compares the fs-LDPI mass spectrum of carbamazepine with the EI-mass spectrum from the NIST library. Both fs-LDPI- and EI-mass spectra display an intact precursor ion at m/z 236. The fragmentation pathway of carbamazepine is straightforward for fs-LDPI- and EI-mass spectra, with the fragmentation patterns described by the inset structure. The primary fragment ions observed are those associated with the iminostilbene (m/z 193) and in the case of fs-LDPI-MS, isocyanic acid (m/z 43). The iminostilbene base peak is produced by the loss of isocyanic acid from the intact precursor.[25-27] The excess positive charge distribution on the carbamazepine cation shown in Figure 5 and the delocalization of charge across its central seven-membered ring predicts the observed stability of the fused ring overall in carbamazepine upon 7.9 eV single photon ionization.

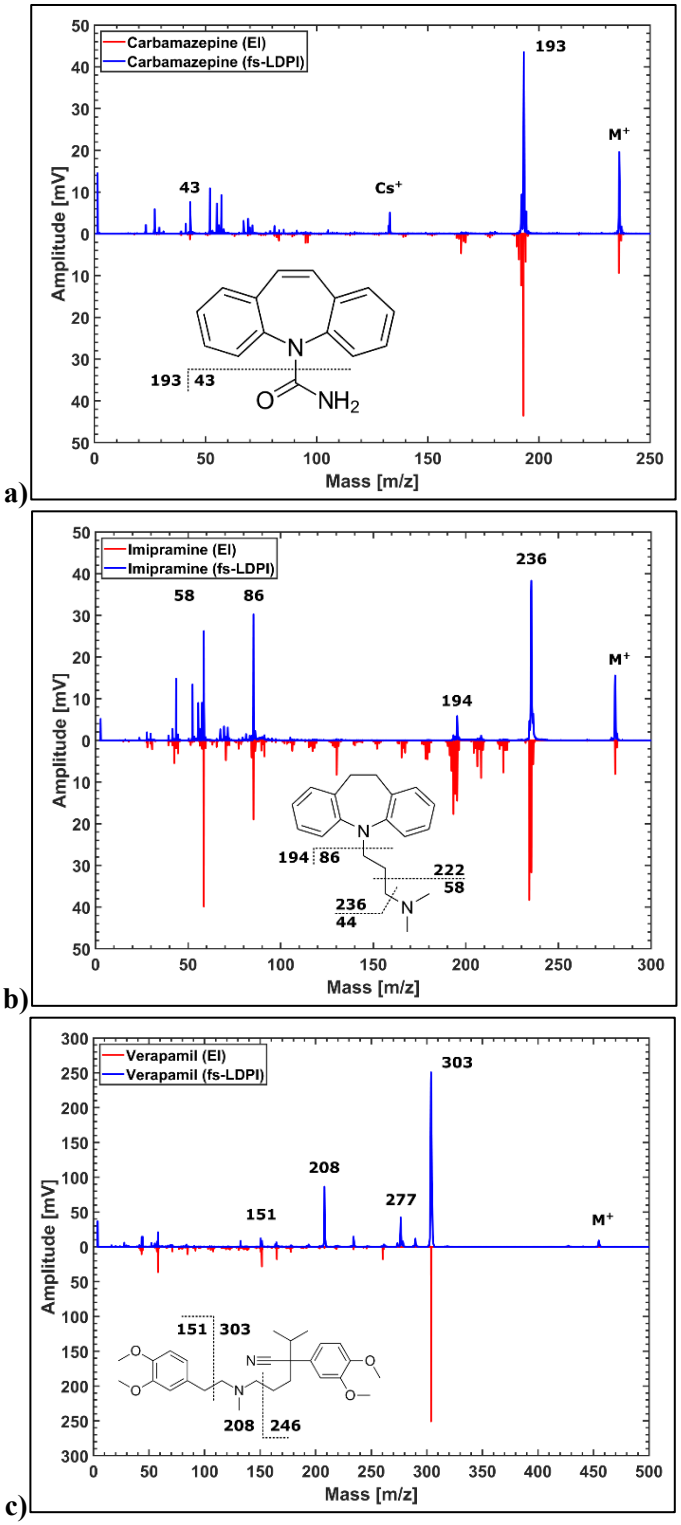

Figure 4. *The positive ion fs-LDPI- and EI-mass spectra for a) carbamazepine, b) imipramine, and c) verapamil (EI-mass spectra normalized to fs-LDPI-MS). No spectra are plotted for ciprofloxacin as no positive ion fs-LDPI-MS was observed for this compound (see text).*

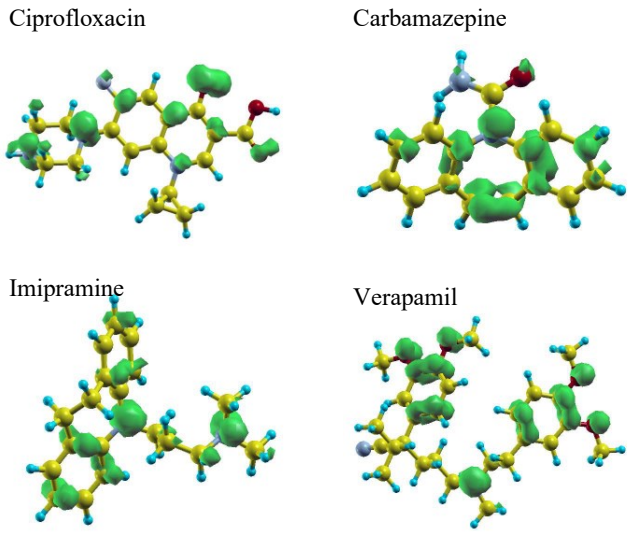

Figure 5. *Real space change in charge density iso-surface of the difference in charge density distribution between the neutral and intact radical cation for each of the four labelled molecules. The green regions indicate the distribution of the positive charge on the molecule. Carbon atoms are yellow, hydrogen atoms are blue, nitrogen atoms are grey, and oxygen atoms are red.*

The overall fragmentation pattern for fs-LDPI-MS of imipramine in Figure 4(b) replicates the most intense fragments from EI-mass spectra, as observed above for carbamazepine. Fused ring stabilization also appeared to occur for imipramine, as both the fs-LDPI- and EI-mass spectra display a prominent precursor peak at m/z 280. The most noteworthy fragment in fs-LDPI-MS appears at m/z 236 and results from the loss of dimethylamine, also very prominent in the EI-mass spectra. The difference in calculated charge density on the terminal nitrogen (at the end of the alkyl chain) shown for imipramine in Figure 5 appears to have initiated an alpha bond cleavage that leads to the formation of the m/z 236 fragment. The m/z 58 peak associated with the dimethylformimine fragment is also relatively intense in both spectra and results from a bond cleavage on the carbon bond beta to the dimethylamine.[28-33] However, while the counterpart ion to m/z 58 is observed in EI-MS at m/z 222, the latter is absent from the fs-LDPI-MS, perhaps due to the overall higher energy available in EI-mass spectra. The m/z 86 and 194 ions observed in both fs-LDPI- and EI-mass spectra result from a bond cleavage between the ring nitrogen and the

first carbon of the sidechain. The tricyclic ring (iminodibenzyl nucleus) retains the positive charge in m/z 194, and the lost sidechain retains the charge in the m/z 86 ion.

Verapamil was observed to fragment in a mode generally similar to that of carbamazepine and imipramine, as shown in Figure 4(c). The most distinct observation is that the intensity of the precursor ion was small in fs-LDPI-MS of verapamil compared to that observed for both carbamazepine and imipramine. However, the low intensity of the verapamil precursor ion in fs-LDPI-MS compares favourably with EI-mass spectra, where it is entirely absent. The relatively high precursor ion signal for all three compounds compared to EI-mass spectra represents a distinct advantage of fs-LDPI-MS, as the presence of even a weak precursor ion is tremendously useful in the interpretation of mass spectra. The alpha-bond cleavage of the lightest benzyl group results in the base peak of both spectra at m/z 303 and lesser peak at m/z 151, presumably because the benzylic bond also acts as the beta-carbon bond for the amino nitrogen atom.[34-36] As expected, the experimental results suggest that the amine holds the majority of the positive charge (indicated by the low intensity of the m/z 151 fragment). Similar to imipramine, a dimethylformimine (m/z 58) fragment is observed which could have resulted from rearrangement of the primary fragment at m/z 303. Surprisingly, the alpha-bond cleavage of the heaviest benzyl group (m/z 246) resulted in the second most intense fragment for fs-LDPI-MS at m/z 208. However, in contrast to the lightest benzyl group (m/z 151) fragment, here the amine moiety of m/z 208 retains all of the positive charge from the precursor ion. Furthermore, both m/z 208 and 277 observed in fs-LDPI are completely absent in the EI-mass spectra. Unfortunately, the source of the rather significant fragment observed at m/z 277 by (only) fs-LDPI-MS has not been identified.

One of the great conceptual advantages of threshold single photon ionization is the relative simplicity of the process renders it more amenable to modelling by electronic structure

calculations. Only the HOMO and a few nearby occupied molecular orbitals are likely to allow threshold single photon ionization and the positively charged ion can be readily modelled, as is shown here. By contrast many other types of ionization are more difficult to model by calculations such as DFT because they can proceed through many more electronic states (i.e., 70 eV electron impact or multiphoton ionization), rely upon potentially mobile protons (i.e., electrospray ionization), involve additional gas phase collisions (i.e., atmospheric pressure chemical or photoionization), and/or some combination thereof (i.e., SIMS or ambient methods).[37]

The 7.9 eV fs-LDPI mass spectra can be more completely interpreted than their corresponding SIMS, given the computationally tractable ionization event of the former, more straightforward fragmentation pattern, shared fragments with EI-mass spectra, and lower chemical noise. Furthermore, fs-LDPI-MS via 7.9 eV single photon ionization for at least three of the four candidate drug compounds produces mass spectra similar to, but simpler than the corresponding EI-mass spectra. One primary difference is that substantially higher fractions of the intact precursor ions were observed for fs-LDPI-MS compared with EI-mass spectra, simplifying mass spectral interpretation. The identification of metabolites by MS imaging of intact samples is complicated by the fragmentation of precursor ions.[6] One method to achieve such chemical identification in MS is to identify by algorithmically comparing EI-mass spectra of chromatographically separated unknowns to fragmentation patterns of known compounds in an EI-mass spectral database.[38] This method has been used for decades in gas chromatography mass spectrometry because the precursor ions are always radical cations, 70 eV EI-mass spectra are particularly reproducible, and the NIST EI-mass spectral library is exceptionally well curated.[38] Furthermore, computational strategies have been developed to predict the EI-mass spectral fragmentation pattern of molecular structures that have not been measured experimentally.[39,40]

However, a wider array of compounds must be tested before EI-mass spectra can be reliably used to predict fs-LDPI-MS.

Acknowledgements

LH was supported by grant CHE-1904145 from the U.S. National Science Foundation. RCW and LH acknowledge the assistance of Igor V. Veryovkin, Jason M. Gross, Igor L. Bolotin, and Emil Tripa in the design, construction, and operation of the right angle ion mirror prism and as well as other aspects of the fs-LDPI-MS instrument. CLP and ISG were supported by the OrbiSIMS project in the Life-Science and Health programme of the National Measurement System of the UK Department of Business, Energy and Industrial Strategy (BEIS). IR also acknowledges the support of the UK Department of BEIS.

Disclosure Statement

The authors have no conflicts to disclose.

Supporting Information

Figure S1. fs-LDPI-MS, fs-LD, and 7.9 eV laser postionization only of imipramine.

Figure S2. Mean and distributions of survival yields for 7.9 eV fs-LDPI-MS of imipramine.

Figure S3. fs-LDPI-MS of imipramine for the lowest and highest desorption laser fluences.

Table S1. GGA Kohn-Sham energy differences for the six highest occupied molecular orbitals.

References

(1) Morgan, P.; Van Der Graaf, P. H.; Arrowsmith, J.; Feltner, D. E.; Drummond, K. S.; Wegner, C. D.; Street, S. D. A. Can the flow of medicines be improved? Fundamental pharmacokinetic and pharmacological principles toward improving phase II survival. *Drug Discovery Today* **2012**, *17*, 419-424.

(2) Cook, D.; Brown, D.; Alexander, R.; March, R.; Morgan, P.; Satterthwaite, G.; Pangalos, M. N. Lessons learned from the fate of astrazeneca's drug pipeline: A five-dimensional framework. *Nature Reviews Drug Discovery* **2014**, *13*, 419-431.

(3) Dollery, C. T. Intracellular drug concentrations. *Clinical Pharmacology & Therapeutics* **2013**, *93*, 263-266.

(4) Vorng, J.-L.; Kotowska, A. M.; Passarelli, M. K.; West, A.; Marshall, P. S.; Havelund, R.; Seah, M. P.; Dollery, C. T.; Rakowska, P. D.; Gilmore, I. S. Semiempirical rules to determine drug sensitivity and ionization efficiency in secondary ion mass spectrometry using a model tissue sample. *Analytical Chemistry* **2016**, *88*, 11028-11036.

(5) Gilmore, I. S. Sims of organics - advances in 2D and 3D imaging and future outlook. *Journal of Vacuum Science Technology A* **2013**, *31*, 050819.

(6) Gilmore, I. S.; Heiles, S.; Pieterse, C. L. Metabolic imaging at the single-cell scale: Recent advances in mass spectrometry imaging. *Annual Review of Analytical Chemistry* **2019**, *12*, 201-224.

(7) Nir, E.; Hunziker, H. E.; de Vries, M. S. Fragment-free mass spectrometric analysis with jet cooling/VUV photoionization. *Analytical Chemistry* **1999**, *71*, 1674-1678.

(8) Hanley, L.; Kornienko, O.; Ada, E. T.; Fuoco, E.; Trevor, J. L. Surface mass spectrometry of molecular species. *Journal of Mass Spectrometry* **1999**, *34*, 705-723.

(9) Hanley, L.; Wickramasinghe, R.; Yung, Y. P. Laser sampling combined with laser postionization for mass spectrometry. *Annual Review of Analytical Chemistry* **2019**, *12*, 225-245.

(10) Heeger, M.; Tyler, B. J.; Körsgen, M.; Arlinghaus, H. F. Laser postionization of neutral molecules sputtered using bismuth and argon cluster primary ions. *Biointerphases* **2018**, *13*, 03B412.

(11) Sabbah, H.; Morrow, A. L.; Pomerantz, A. E.; Zare, R. N. Evidence for island structures as the dominant architecture of asphaltenes. *Energy & Fuels* **2011**, *25*, 1597-1604.

(12) Edirisinghe, P. D.; Moore, J. F.; Calaway, W. F.; Veryovkin, I. V.; Pellin, M. J.; Hanley, L. Vacuum ultraviolet postionization of aromatic groups covalently bound to peptides. *Analytical Chemistry* **2006**, *78*, 5876-5883.

(13) Bhardwaj, C.; Cui, Y.; Hofstetter, T.; Liu, S. Y.; Bernstein, H. C.; Carlson, R. P.; Ahmed, M.; Hanley, L. Differentiation of microbial species and strains in coculture biofilms by multivariate analysis of laser desorption postionization mass spectra. *Analyst* **2013**, *138*, 6844-6851.

(14) Akhmetov, A.; Bhardwaj, C.; Hanley, L. Laser desorption postionization mass spectrometry imaging of biological targets, in *Mass spectrometry imaging of small molecules*, He, L., Ed.; *Methods in Molecular Biology*, vol. 1203, Springer Science+Business Media: New York, 2015, pp 185-194.

(15) Schmid, P.; Stöhr, F.; Arndt, M.; Tüxen, J.; Mayor, M. Single-photon ionization of organic molecules beyond 10 kDa. *Journal of the American Society for Mass Spectrometry* **2013**, *24*, 602-608.

(16) Cui, Y.; Bhardwaj, C.; Milasinovic, S.; Carlson, R. P.; Gordon, R. J.; Hanley, L. Molecular imaging and depth profiling of biomaterials interfaces by femtosecond laser desorption postionization mass spectrometry. *ACS Applied Materials & Interfaces* **2013**, *5*, 9269-9275.

(17) Cui, Y.; Veryovkin, I. V.; Majeski, M. W.; Cavazos, D. R.; Hanley, L. High lateral resolution vs. Molecular preservation in near-IR fs-laser desorption postionization mass spectrometry. *Analytical Chemistry* **2015**, *87*, 367-371.

(18) Gross, J. M.; Hanley, L.; Veryovkin, I. V. Comparing flat-top and Gaussian femtosecond laser ablation of silicon at normal and oblique angles of incidence, in *Proc. of SPIE Laser Beam Shaping XIX*; 11107, SPIE, **2019**, 111070I.

(19) Cui, Y.; Moore, J. F.; Milasinovic, S.; Liu, Y.; Gordon, R. J.; Hanley, L. Depth profiling and imaging capabilities of an ultrashort pulse laser ablation time of flight mass spectrometer. *Review of Scientific Instruments* **2012**, *83*, 093702.

(20) Veryovkin, I. V.; Hanley, L. Right angle ion mirror-prism (RAIMP): Mass analyzer combining slit spectroscopy with retarding electric field, in *Proc. of 65th ASMS Conference on Mass Spectrometry and Allied Topics*; American Society of Mass Spectrometry: Indianapolis, IN, 2017.

(21) Veryovkin, I. V.; Hanley, L. Multimode ion mirror prism and energy filtering apparatus and system for time-of-flight mass spectrometry, US Patent No. 10,622,203 B2, **2020**.

(22) Soler, J. M.; Artacho, E.; Gale, J. D.; García, A.; Junquera, J.; Ordejon, P.; Portal, D. S. The siesta method for ab initio order-n materials simulation. *Journal of Physics: Condensed Matter* **2002**, *14*, 2745.

(23) Droghetti, A.; Rungger, I.; Das Pemmaraju, C.; Sanvito, S. Fundamental gap of molecular crystals via constrained density functional theory. *Physical Review B* **2016**, *93*, 195208.

(24) Akhmetov, A.; Moore, J. F.; Gasper, G. L.; Koin, P. J.; Hanley, L. Laser desorption postionization for imaging MS of biological material. *Journal of Mass Spectrometry* **2010**, *45*, 137-145.

(25) Frigerio, A.; Fanelli, R.; Biandrate, P.; Passerini, G.; Morselli, P. L.; Garattini, S. Mass spectrometric characterization of carbamazepine-10,11-epoxide, a carbamazepine metabolite isolated from human urine. *Journal of Pharmaceutical Sciences* **1972**, *61*, 1144-1147.

(26) Palmér, L.; Bertilsson, L.; Coliste, P.; Rawlins, M. Quantitative determination of carbamazepine in plasma by mass fragmentography. *Clinical Pharmacology & Therapeutics* **1973**, *14*, 827-832.

(27) Baker, K. M.; Frigerio, A. Loss of hydrogen cyanide and dihydrogen cyanide radical from aromatic nitrogen heterocycles on electron impact. *Journal of the Chemical Society, Perkin Transactions 2* **1973**, 648-649.

(28) Frigerio, A.; Belvedere, G.; De Nadai, F.; Fanelli, R.; Pantarotto, C.; Riva, E.; Morselli, P. L. A method for the determination of imipramine in human plasma by gas-liquid chromatography-mass fragmentography. *Journal of Chromatography A* **1972**, *74*, 201-208.

(29) Claeys, M.; Muscettola, G.; Markey, S. P. Simultaneous measurement of imipramine and desipramine by selected ion recording with deuterated internal standards. *Biomed Mass Spectrom* **1976**, *3*, 110-116.

(30) Biggs, J. T.; Holland, W. H.; Chang, S.; Hipps, P. P.; Sherman, W. R. Electron beam ionization mass fragmentographic analysis of tricyclic antidepressants in human plasma. *Journal of Pharmaceutical Sciences* **1976**, *65*, 261-268.

(31) Alkalay, D.; Volk, J.; Carlsen, S. A sensitive method for the simultaneous determination in biological fluids of imipramine and desipramine or clomipramine and n-desmethylclomipramine by gas chromatography mass spectrometry. *Biomedical mass spectrometry* **1979**, *6*, 200-204.

(32) Suzuki, O.; Hattori, H.; Asano, M.; Brandenberger, H. Positive and negative ion mass spectrometry of tricyclic antidepressants. *Zeitschrift für Rechtsmedizin* **1986**, *97*, 239-250.

(33) Fujii, T.; Kurihara, Y.; Arimoto, H.; Mitsutsuka, Y. Surface ionization organic mass spectrometry of imipramine, desipramine, clomipramine, and lidocaine. *Analytical Chemistry* **1994**, *66*, 1884-1889.

(34) Eichelbaum, M.; Ende, M.; Remberg, G.; Schomerus, M.; Dengler, H. J. The metabolism of DL-[14C]verapamil in man. *Drug Metabolism and Disposition* **1979**, *7*, 145-148.

(35) Rustichelli, C.; Ferioli, V.; Gamberini, G. Resolution of the enantiomers of verapamil and gallopamil by chiral liquid chromatography-mass spectrometry. *Chromatographia* **1997**, *44*, 477-483.

(36) Vaikkinen, A.; Shrestha, B.; Kauppila, T. J.; Vertes, A.; Kostiainen, R. Infrared laser ablation atmospheric pressure photoionization mass spectrometry. *Analytical Chemistry* **2012**, *84*, 1630-1636.

(37) Bhardwaj, C.; Hanley, L. Ion sources for mass spectrometric identification and imaging of molecular species *Natural Product Reports* **2014**, *31*, 756-767.

(38) Stein, S. Mass spectral reference libraries: An ever-expanding resource for chemical identification. *Analytical Chemistry* **2012**, *84*, 7274-7282.

(39) Allen, F.; Pon, A.; Greiner, R.; Wishart, D. Computational prediction of electron ionization mass spectra to assist in GC/MS compound identification. *Analytical Chemistry* **2016**, *88*, 7689-7697.

(40) Wei, J. N.; Belanger, D.; Adams, R. P.; Sculley, D. Rapid prediction of electron–ionization mass spectrometry using neural networks. *ACS Central Science* **2019**, *5*, 700-708.

Supporting Information for

An Experimental and Theoretical Study of Laser Postionization of Femtosecond Laser Desorbed Drug Molecules

Cornelius L. Pieterse, Ivan Rungger, and Ian S. Gilmore
National Physical Laboratory, Hampton Road, Teddington, TW11 0LW UK
Raveendra C. Wickramasinghe and Luke Hanley*
Department of Chemistry, University of Illinois at Chicago, Chicago, IL 60607 USA
Corresponding author email: LHanley@uic.edu

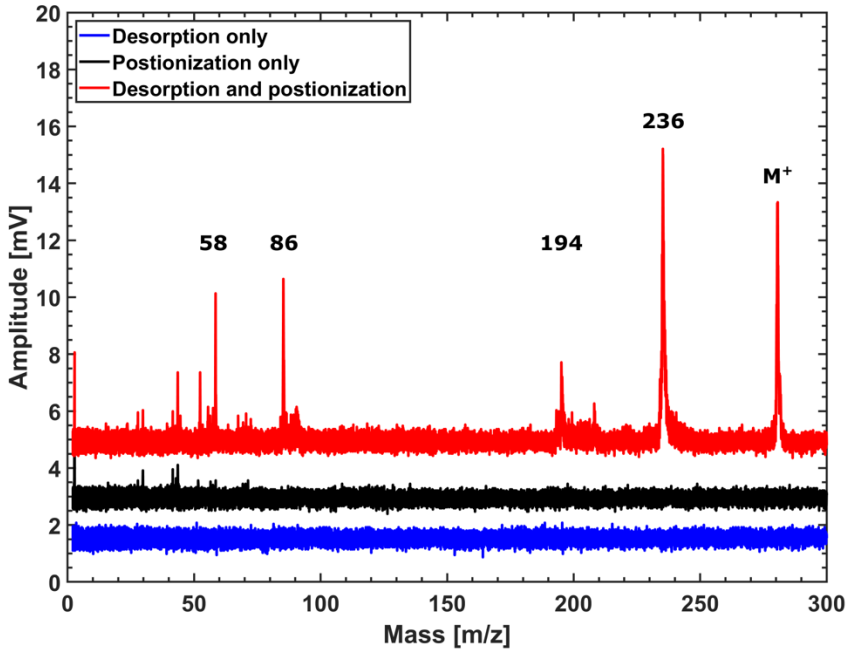

Figure S1*. fs-LDPI-MS (red), fs-LDI (blue), and 7.9 eV laser postionization (black) only of imipramine.*

Impact of desorption laser fluence on fragmentation. The primary focus of this work is to explore threshold single photon ionization of neutral drug molecules in the gas-phase. However, it is also useful to explore the unique characteristics of using fs-laser desorption (fs-LD) to volatilize these molecules. The same methodology was followed here as described in previous studies:[1,2] the survival yields were calculated as $S = I_M/(I_M + I_F)$, where I_M and I_F are the integrated abundances of the molecular and fragment ion intensities, respectively. The mean survival yields were determined by averaging the survival yield distributions and assumes that all ions have the same detection efficiency.[3] The overall softness of the desorption process was determined here by measuring the survival yield as a function of desorption laser fluence. The concept of using survival yields assumes that a single unimolecular dissociation is represented by

the mass spectrum. Figure S2 shows the survival yields for imipramine during fs-LDPI-MS, where (top) shows the survival yield as a function of fluence, and (bottom) shows the survival yield distribution for the highest fluence measured. The measurement repeatability was determined by calculating the average signal intensity I and survival yields S of five carbamazepine samples ($I = 56 \pm 12$ mV and $S = 0.47 \pm 0.07$). It is well-established that even for samples which are prepared in the same fashion, there tends to be considerable variability in the absolute signal intensity of nanosecond laser desorption/ionization.[4,5]

There have been only a limited number of studies investigating the application of femtosecond pulses for desorption/ablation in MS imaging.[6-11] The most striking observation here is that, for the fluence range studied, the fragmentation did not change with desorption laser fluence, staying constant at $S \sim 0.26$. The survival yield histogram structure, also shown in Figure S2 (top), indicated a fluence independence that would enhance measurement repeatability. Although signal intensity variations for each individual measurement (sample) were observed, the variability of the mean for the different measurements was acceptable (standard Gaussian statistics are used to calculate the error bars). Prior results for 800 nm fs-LD found ranges of laser fluence over which survival yields were relatively constant,[7] but the survival yields did eventually vary at sufficiently low or high fluences.[7,9] Prior work has shown the ability of fs-LDPI-MS (using 10.5 eV single photon ionization) and fs-LDI-MS (without using postionization) to transfer similar amounts of internal energy to a precursor ion as vacuum-based matrix assisted laser desorption ionization MS.[7] Other aspects of the fs-LD process and how it can be coupled to single photon ionization for fs-LDPI-MS imaging have been discussed elsewhere.[8,9,11] Overall, the results of Figure S2 are intriguing, given that nanosecond pulsed laser-based desorption techniques typically depend nonlinearly on laser fluence.[12,13] Nevertheless, further experiments are required to explore the dependence of fragmentation on laser fluence in fs-LD and its impact on shot-to-shot reproducibility.

Many of the peaks between m/z 50 and 60 in the 7.9 eV fs-LDPI-MS of Figure 3\4 are from the underlying metal substrate while a Cs^+ peak shown in Figure 4(a) arose from the presence of added CsI calibrant. This can be seen in the mass spectra in Figure S3 in which an enhancement of ion signals is associated with the stainless-steel substrate at high laser fluence, consistent with an earlier study.[9]

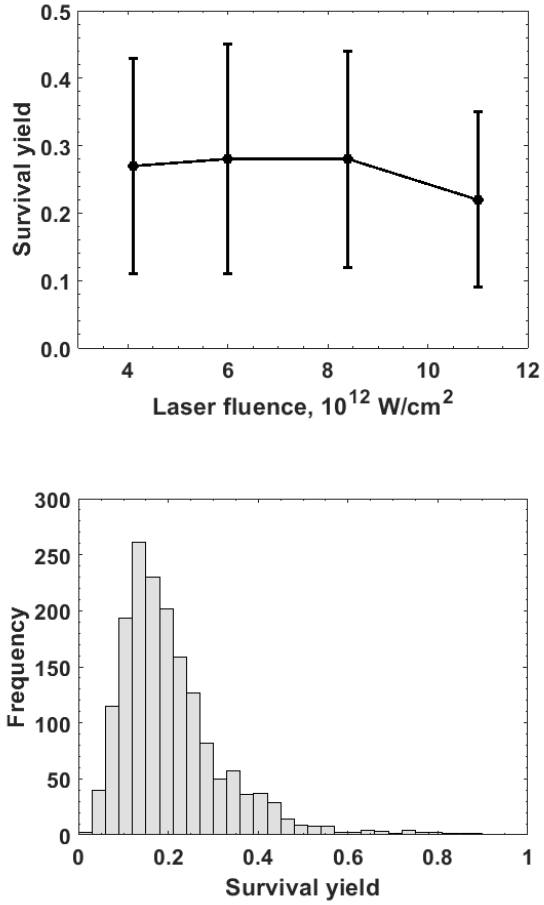

Figure S2. *(Top) Mean survival yield for the fluence range studied for 7.9 eV fs-LDPI-MS of imipramine. (Bottom) Survival yield distribution of imipramine for the highest fluence* (1.1×10^{13} *W/cm*^{2}*).*

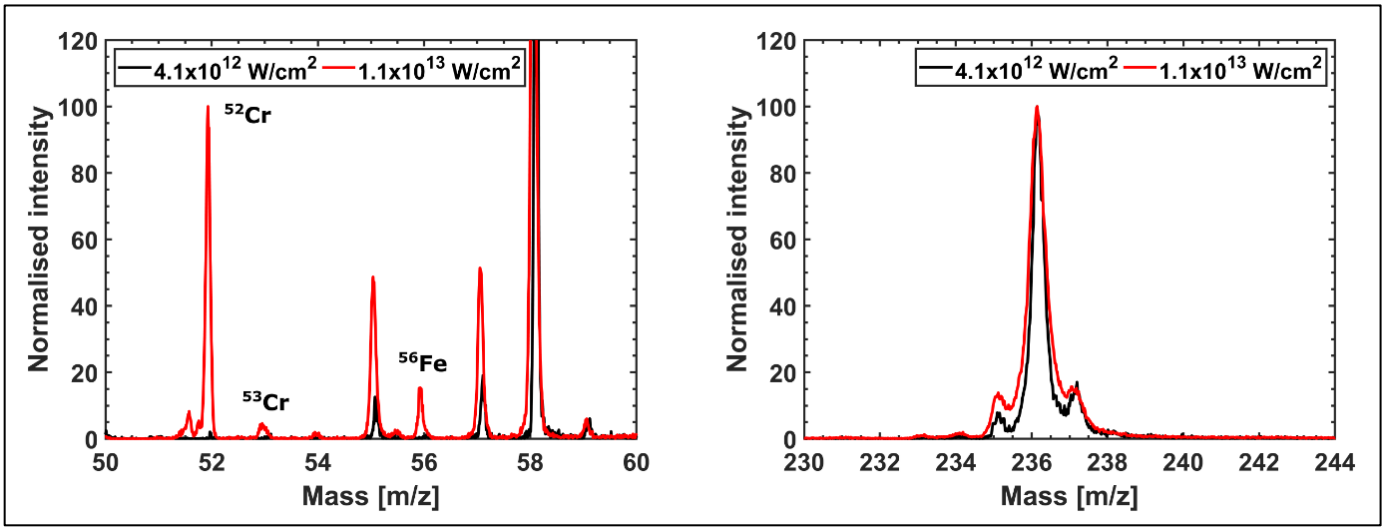

Figure S3. *fs-LDPI-MS of imipramine for the lowest and highest desorption laser fluences (*4.1×10^{12} W/cm^2 *and* 1.1×10^{13} W/cm^2*) emphasizing peaks originating from the stainless-steel substrate (left) and a fragment of imipramine (right).*

Table S1. GGA Kohn-Sham energy differences for the six highest occupied molecular orbitals (HOMOs).

	Carbamazepine	Ciprofloxacin	Verapamil	Imipramine
E_{HOMO}-E_{HOMO-1}(eV)	0.16	0.31	0.08	0.45
E_{HOMO}-E_{HOMO-2}(eV)	0.51	0.54	0.19	1.36
E_{HOMO}-E_{HOMO-3}(eV)	0.82	0.63	0.91	1.51
E_{HOMO}-E_{HOMO-4}(eV)	1.09	1.00	1.06	1.63
E_{HOMO}-E_{HOMO-5}(eV)	1.37	1.57	2.36	2.28

Comparison of Highest and Nearby Occupied Molecular Orbitals. Density functional theory (DFT) was performed with the semi-local exchange correlation functionals GGA and LDA. The negative of the Kohn-Sham energy eigenvalue for the highest occupied molecular orbital (HOMO) - E_{HOMO} - typically underestimates the experimental ionization energy (IE) such that $E_{HOMO} < IE$. However, the shape of the HOMO wave function is usually captured correctly by this procedure. Thus, the shape of the HOMO wavefunctions in Figure 3 are generally accurate, but the relative energy differences between HOMO and HOMO-1, as shown in Table S1, are underestimated.

References for Supporting Information

(1) Luo, G.; Marginean, I.; Vertes, A. Internal energy of ions generated by matrix-assisted laser desorption/ionization. Analytical Chemistry **2002**, 74, 6185-6190.

(2) Luo, G.; Marginean, I.; Ye, L.; Vertes, A. Competing ion decomposition channels in matrix-assisted laser desorption ionization. *The Journal of Physical Chemistry B* **2008**, *112*, 6952-6956.

(3) Gilmore, I.; Seah, M. P. Ion detection efficiency in SIMS: Dependencies on energy, mass and composition for microchannel plates used in mass spectrometry. *International Journal of Mass Spectrometry* **2000**, *202*, 217-229.

(4) Vorm, O.; Roepstorff, P.; Mann, M. Improved resolution and very high sensitivity in MALDI ToF of matrix surfaces made by fast evaporation. *Analytical Chemistry* **1994**, *66*, 3281-3287.

(5) Ahn, S.; Park, K.; Bae, Y.; Kim, M. Efficient methods to generate reproducible mass spectra in matrix-assisted laser desorption ionization of peptides. *Journal of the American Society for Mass Spectrometry* **2013**, *24*, 868-876.

(6) Flanigan, P.; Levis, R. Ambient femtosecond laser vaporization and nanosecond laser desorption electrospray ionization mass spectrometry. *Annual Review of Analytical Chemistry* **2014**, *7*, 229-256.

(7) Milasinovic, S.; Cui, Y.; Gordon, R. J.; Hanley, L. Internal energy of thermometer ions formed by femtosecond laser desorption: Implications for mass spectrometric imaging. *Journal of Physical Chemistry C* **2014**, *118*, 28938-28947.

(8) Cui, Y.; Bhardwaj, C.; Milasinovic, S.; Carlson, R. P.; Gordon, R. J.; Hanley, L. Molecular imaging and depth profiling of biomaterials interfaces by femtosecond laser desorption postionization mass spectrometry. *ACS Applied Materials & Interfaces* **2013**, *5*, 9269-9275.

(9) Cui, Y.; Veryovkin, I. V.; Majeski, M. W.; Cavazos, D. R.; Hanley, L. High lateral resolution vs. molecular preservation in near-IR fs-laser desorption postionization mass spectrometry. *Analytical Chemistry* **2015**, *87*, 367-371.

(10) Walker, A. V.; Gelb, L. D.; Barry, G. E.; Subanajouy, P.; Poudel, A.; Hara, M.; Veryovkin, I. V.; Bell, G. I.; Hanley, L. Femtosecond laser desorption ionization mass spectrometry imaging and multivariate analysis of lipids in pancreatic tissue. *Biointerphases* **2018**, *13*, 03B416.

(11) Hanley, L.; Wickramasinghe, R.; Yung, Y. P. Laser sampling combined with laser postionization for mass spectrometry. *Annual Review of Analytical Chemistry* **2019**, *12*, 225-245.

(12) Dreisewerd, K.; Schürenberg, M.; Karas, M.; Hillenkamp, F. Influence of the laser intensity and spot size on the desorption of molecules and ions in matrix-assisted laser desorption/ionization with a uniform beam profile. *International Journal of Mass Spectrometry and Ion Processes* **1995**, *141*, 127-148.

(13) Dreisewerd, K. Recent methodological advances in MALDI mass spectrometry. *Analytical and Bioanalytical Chemistry* **2014**, *406*, 2261-2278.